Materials Science and Engineering C 51 (2015) 16–27

Contents lists available at ScienceDirect

Materials Science and Engineering C

journal homepage: www.elsevier.com/locate/msec

Nanofibrous yet injectable polycaprolactone-collagen bone tissue scaffold with osteoprogenitor cells and controlled release of bone morphogenetic protein-2

Gayathri Subramanian [a], Callan Bialorucki [a], Eda Yildirim-Ayan [a,b,*]

[a] Department of Bioengineering, College of Engineering, University of Toledo, Toledo, OH 43606, USA
[b] Department of Orthopaedic Surgery, University of Toledo Medical Center, Toledo, OH 43614, USA

ARTICLE INFO

Article history:
Received 30 October 2014
Received in revised form 21 January 2015
Accepted 23 February 2015
Available online 25 February 2015

Keywords:
Injectable scaffold
BMP-2 release
Osteogenic differentiation
Polycaprolactone
Collagen type-I

ABSTRACT

In this work, we developed a nanofibrous, yet injectable orthobiologic tissue scaffold that is capable of hosting osteoprogenitor cells and controlling kinetic release profile of the encapsulated pro-osteogenic factor without diminishing its bioactivity over 21 days. This innovative injectable scaffold was synthesized by incorporating electrospun and subsequently O_2 plasma-functionalized polycaprolactone (PCL) nanofibers within the collagen type-I solution along with MC3T3-E1 cells (pre-osteoblasts) and bone morphogenetic protein-2 (BMP2). Through changing the PCL nanofiber concentration within the injectable scaffolds, we were able to tailor the mechanical strength, protein retention capacity, bioactivity preservation, and osteoinductive potential of the scaffolds. The nanofibrous internal structure of the scaffold allowed us to use a low dose of BMP2 (200 ng/ml) to achieve osteoblastic differentiation in *in vitro* culture. The osteogenesis capacity of the injectable scaffolds were evaluated though measuring MC3T3-E1 cell proliferation, ALP activity, matrix mineralization, and early- and late-osteoblast specific gene expression profiles over 21 days. The results demonstrated that the nanofibrous injectable scaffold provides not only an osteoinductive environment for osteoprogenitor cells to differentiate, but also a suitable biomechanical and biochemical environment to act as a reservoir for osteogenic factors with controlled release profile.

1. Introduction

About 2 million cases of trauma or disease-related bone fractures occur every year in the US alone, with an annual direct cost of $10 billion [1]. Bone grafts (auto- and allografts) have primarily been employed in bone fracture treatment when the defect exceeds the body's inherent bone healing capacity. However, limited availability of autografts and possible disease transmission from allografts are major restraints [2–4]. Furthermore, bone grafts cannot be employed for irregular-shaped bone fractures due to their solid structures. Bone filler materials such as polymethylmethacrylate (PMMA) and calcium phosphate-based resins have been utilized as an alternative to bone grafts due to their injectability, inexpensive synthesis processes, and immediate fracture stabilization feature. These injectable bone filler materials; however, have exothermic polymerization processes and limited regenerative potential [5–7]. They are, thus unable to deliver biologics (cells, proteins/growth factors) and induce regeneration of bone tissue in the defect area. Consequently, research has focused on bone filler materials that have both osteoinductive properties similar to autografts and injectable properties similar to PMMA, yet that are able to deliver biological factors for osteogenesis and possess three dimensional structure for bone regeneration.

Bone morphogenetic proteins (BMPs) are pro-osteogenic factors that play a prominent role in recruiting osteoprogenitor cells, inducing terminal differentiation into functional osteoblasts and expediting bone formation *in vivo* [8–10]. Native BMP2 and its recombinant equivalents, in specific, are known to stimulate proliferation and differentiation in cells and increase alkaline phosphatase (ALP), osteocalcin, and collagen type-I gene expression levels in mesenchymal stem cells [11], C2C12 cells [12] and MC3T3-E1 [13]. Effective administration of BMP2; however, is challenging because of its short half-life (90 min), decreased bioactivity, and burst release [14]. To ensure that there is enough BMP2 remaining at the treatment site to have any therapeutic effect, BMP2 dosage of more than 100-fold of physiological concentration has to be introduced in the bone scaffolds. However, higher than natural BMP2 dosage (around 5 μg) leads to undesirable cytotoxic and inflammatory effects, increased osteoclastic activity (bone resorption), uncontrolled ectopic bone formation, and carcinoma [15–17]. Based on *in vitro* and *in vivo* studies, a low dose of BMP2 with a sustained release profile has been found optimal for osteogenesis [18–20]. Thus, there is a great need for a BMP2-encapsulated bone scaffold that is able to both retain the growth factor and preserve its bioactivity

* Corresponding author at: Department of Bioengineering, College of Engineering, University of Toledo, Toledo, OH 43606, USA.
E-mail address: eda.yildirimayan@utoledo.edu (E. Yildirim-Ayan).

http://dx.doi.org/10.1016/j.msec.2015.02.030
0928-4931/

for the duration necessary to attain conductive environment for osteogenesis.

In an effort to achieve sustained release profile of growth factors, protein encapsulation techniques have been investigated. Microspheres and nanoparticles that act as BMP2 carriers within injectable scaffolds slow down the protein release rate from the construct [21–24]. BMP2-loaded polymeric microspheres incorporated into injectable calcium phosphate ceramics have showed favorable release profiles with prolonged activity of the protein [22]. HA nanoparticles encapsulated with BMP2 within the chitosan hydrogels [23] and PLGA/HA composite scaffolds [24] also enhanced the osteoinductivity of the respective materials. Despite promising results, the limitations noticed with such encapsulation techniques are initial burst release and decreased bioactivity of encapsulated proteins due to the organic solvents used in microsphere and nanoparticle fabrication [25,26]. Thus, growth factors subjected to harsh organic solvents during microsphere/scaffold synthesis were blended with bovine serum albumin (BSA) prior to encapsulation in order to provide a protective shell around the protein and subsequently preserving its bioactivity [17,27]. Heparin, a hyper-sulfated glycosaminoglycan is also known to have high affinity to growth factors [28,29], was reported to extend the half-life of BMP2 by more than 20-fold *in vitro* [30].

The objectives of this study were 1) to create an injectable nanofibrous bone tissue scaffold through incorporating PCL nanofibers into collagen type-1 with osteoprogenitor cells and recombinant human BMP2 and 2) to study how PC nanofiber concentration affect encapsulated protein retention rate, protein's bioactivity, injectable scaffold's viscoelastic properties, and osteoinductive capacity for bone repair and regeneration. We hypothesized that the nanofibrous structure of the PCL is ideal for immobilizing BMP2 to enhance protein retention, while heparin/BSA solution is required for enhanced bioactivity. We have tested our hypothesis through (a) characterizing the mechanical and biological properties of the scaffold with varying concentrations of PCL nanofibers, (b) evaluating the performance of the biomolecules heparin and BSA in maintenance of BMP2 activity, and (c) investigating the long-term *in vitro* osteoinductive potential of the scaffold in terms of proliferation, alkaline phosphatase levels, matrix mineralization, and osteoblast-specific gene expression profiles of cells encapsulated within the scaffold.

2. Materials and methods

2.1. Synthesis of the nanofibrous and injectable orthobiologic biomaterial

The nanofibrous and injectable orthobiologic biomaterial was fabricated through interspersing PCL electrospun nanofibers within the collagen type-I, osteoprogenitor cells, and pro-osteogenic factor loaded solution. This orthobiologic injectable yet nanofibrous scaffold, called BMP2/*hb*-PNCOL, was synthesized by following three major sequential steps explained below. Fig. 1 illustrates the overall experimental procedure in synthesizing the injectable BMP2/*hb*-PNCOL scaffold.

A) Polycaprolactone (PCL) nanofiber fabrication and functionalization
PCL nanofibers were fabricated by the electrospinning PCL (Mw = 45,000, Sigma-Aldrich) dissolved in an organic solvent mixture using our established protocol [31]. Briefly, a 16% (w/v) solution of PCL dissolved in a solvent mixture with 3:1 volume ratio of chloroform/methanol was delivered *via* a syringe pump at a feed rate of 8000 μl/h with 20 KV voltage supply. The fibers collected on the aluminum foil plate were dried for 72 h, peeled off as a mat and carefully cut into pieces. These pieces were further chopped using a high speed homogenizer (Ultra Turrax) to obtain tiny fragments of electrospun mats that still retained their nanofibrous structure. The fibers were then subjected to oxygen-based plasma treatment (Harrick Plasma) for 3 min to introduce functional groups on the surface of PCL and reduce its hydrophobicity [32].

B) Neutralized collagen type-I solution preparation and cell seeding within the scaffold
Collagen type-I (BD Biosciences, USA) solution at 4.41 mg/ml concentration and pH ~ 3–4 was diluted to 2.5 mg/ml and neutralized with chilled 1 N NaOH along with phosphate buffer saline (PBS) and deionized water according to manufacturer's protocol. Finely cut pieces of electrospun PCL nanofibers mats were functionalized and added into the polymerizing collagen solution at 0%, 1%, 3%, 6% (w/v) concentration to prepare injectable PCL-collagen (PNCOL) scaffolds. The fine size of PCL nanofibers allowed us to mix the PNCOL solution homogenously using a pipette prior to addition of cells and pro-osteogenic factor.

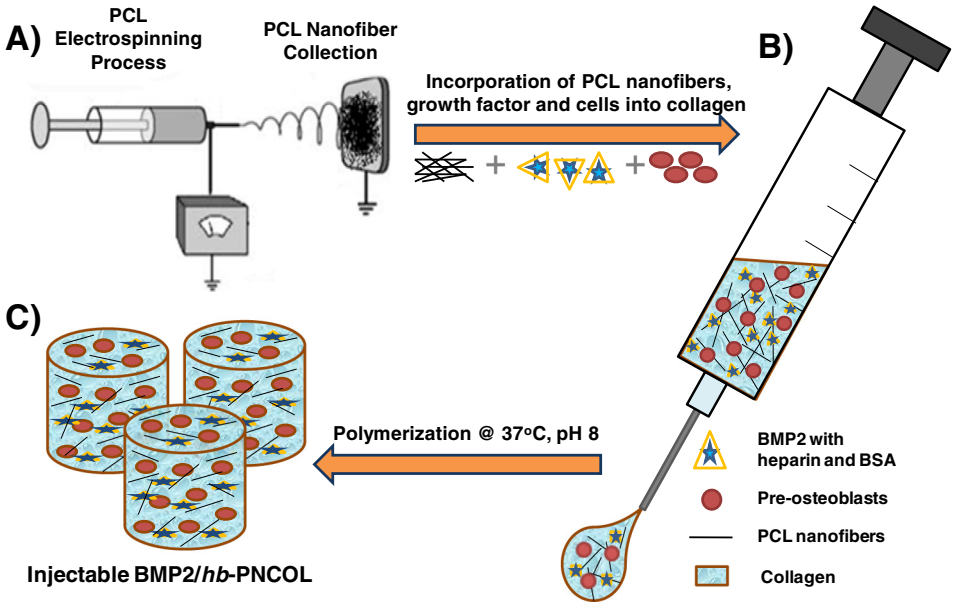

Fig. 1. Synthesis of the injectable orthobiologic scaffold. (A) PCL nanofibers were obtained through electrospinning technique. (B) Collagen solution was neutralized and 200 ng/ml BMP2 was blended with heparin and BSA at 1:40:2000 ratio to preserve and enhance BMP2 activity. Osteoprogenitor cells, BMP2 with heparin and BSA and functionalized PCL nanofibers were admixed with the neutralized 2.5 mg/ml collagen type-I solution. C) Nanofibrous and injectable scaffold, BMP2/*hb*-PNCOL, was transferred to incubator for further polymerization.

Pre-osteoblastic cells MC3T3-E1 (ATCC, CRL-2593; USA) between passages 3–5 were incorporated in the neutralized PCL-collagen solution at $1x10^6$ cells/ml seeding density. Prior incorporation within the scaffolds, cells were maintained in complete media comprising of Alpha-Minimum Essential Medium (α-MEM) (Life Technologies, USA) supplemented with 10% Fetal Bovine Serum (Gibco, USA) and 1% Penicillin–Streptomycin (Life Technologies, USA). For long-term *in vitro* study, scaffolds were incubated within osteogenic media prepared by adding osteogenic factors (10 mM ß-glycerophosphate (Sigma-Aldrich, US) and 50 μg/ml ascorbic acid (Sigma-Aldrich, US) into the complete media.

C) Pro-osteogenic factor incorporation within nanofibrous injectable scaffold

Recombinant human Bone Morphogenetic Protein 2 (BMP2; Peprotech, USA) was used as a pro-osteogenic factor in this study. BSA (Sigma-Aldrich, US) and heparin (Sigma-Aldrich, US) were employed to protect BMP2 from degradation and prolong its bioactivity. BMP2 was incubated with heparin (*h*) and then BSA (*b*) at a ratio of 1:40:2000, respectively for 15 min at room temperature to prepare BMP2/*h*b-PNCOL scaffolds. Unless otherwise specified, 200 ng/ml of BMP2 was incorporated in the scaffold solution. Scaffolds were then transferred to the incubator to allow further polymerization, and subsequently cultured in complete media unless otherwise mentioned, with the media being replaced every 3–4 days. Four samples (n = 4) were used for each condition for all assays, unless stated otherwise.

2.2. Morphology, mechanical properties, protein retention, and protein activity of the injectable orthobiologic scaffold

2.2.1. Studying external and internal morphology of injectable scaffold

The morphological changes following PCL nanofiber incorporation were investigated using scanning electron microscopy (SEM) and surface area and porosimetry analyzer. SEM micrographs provided morphological and porosity changes on the scaffold surface, while data from the surface area analyzer provided the internal morphological changes within the scaffold upon PCL nanofiber introduction. For SEM, 0%, 1%, 3% and 6% (w/v) PNCOL scaffolds were synthesized, frozen in liquid nitrogen and transferred to a freeze-dryer (Freezone system, Labconco®) to ensure complete dehydration. The dried scaffolds were viewed under SEM (Quanta™ 3D FEG) at 10KV excitation energy.

For surface area measurements, 1 g of the freeze-dried samples (n = 6) were degassed at 40 °C for 16 h and analyzed using surface area and porosity analyzer (Micromeritics ASAP 2020) to obtain N_2 adsorption and desorption isotherms of each sample. The analyzer (Micromeritics ASAP 2020, Inc.) was capable of detecting surface features and pore sizes above 500 nm [33]. Thus, in this study, surface features below 500 nm were not considered in surface area determination. Brunauer–Emmett–Teller (BET) technique was employed to perform internal surface area calculations using N2 adsorption and desorption isotherms data from the analyzer.

2.2.2. Measuring viscoelastic properties of injectable scaffold

To determine the elastic and viscous properties of the scaffolds, rheological analysis (n = 6) was conducted using a parallel plate rheometer (Rheometric Scientific). PNCOL solutions with specified PCL nanofiber concentrations were prepared and polymerized in 35 mm petridishes at 37 °C. Cylindrical samples (2 mm height) were placed between the parallel plates made of nonporous metal. The top plate was lowered to a gap distance of 0.5 mm and frequency sweep test ranging from 1 to 100 rad/s was performed at 20% strain under dynamic conditions. Rheological measurements provided the storage modulus (G') and the loss modulus (G'') as a function of frequency at a fixed temperature using RDA software (TA instruments).

2.2.3. Measuring model protein retention within the injectable scaffold

The short- and long-term protein retention capacity of injectable scaffolds with various PCL nanofiber concentration was investigated with 0%, 1%, 3% and 6% (w/v) PNCOL scaffolds through measuring the release profile of a model protein over 4 h and over 21 days, respectively. Lysozyme was used as a model protein because its physicochemical properties and size are similar to many growth factors including BMP2, with a molecular weight of 14.4KDa, isoelectric point (pI 9–10), and molar extension coefficient around 38,000 cm^{-1} M^{-1} [34]. Lysozyme (MW 14,500, Sigma-Aldrich) was covalently labeled with Alexa Fluor 350 dye (Molecular Probes) and purified by size exclusion chromatography using Sephadex G-25 resin column (Sigma-Aldrich). The Alexa Fluor 350 tagged lysozyme was incorporated into PNCOL scaffold solutions at a final concentration of 50 μg/ml. The release profile of lysozyme from the PNCOL scaffolds was determined at 1, 2, 3 and 4 h to study the initial burst, followed by 1, 2, 4, 6, 10, 14, 17 and 21 days to study diffusion of protein over a longer period of time by aspirating the supernatant (PBS) from each sample completely, and replacing it with equivalent volume of fresh PBS. The collected samples were transferred into 96-well UV-Plate (Thermo Scientific) and analyzed for fluorescence using a microplate fluorometer (Wallac 1420) at 346 nm excitation and 442 nm emission wavelengths. The amount of lysozyme released at each time point was determined from the standard curve generated by plotting the fluorescence intensities obtained from different known concentrations of the dye-labeled lysozyme.

2.2.4. Measuring BMP2 bioactivity and identifying optimal BMP2 concentration within the injectable orthobiologic scaffold

The various components of the injectable scaffold, such as PCL nanofiber concentration and presence of heparin/BSA might affect the bioactivity of the encapsulated BMP2. To understand the effect of PCL nanofiber concentration on BMP2 activity, BMP2 was incorporated within 0%, 1%, 3% and 6% (w/v) PNCOL scaffolds and ALP activity of MC3T3-E1 cells was measured. To identify the solo and combined effects of heparin and BSA on the BMP2 activity, four groups were used *i*) BMP2-PNCOL (control), *ii*) BMP2/*h*-PNCOL, *iii*) BMP2/*b*-PNCOL, and iv) BMP2/*hb*-PNCOL. In these groups, *h* refers to heparin, while *b* denotes BSA. The bioactivity study was conducted indirectly through measuring the alkaline phosphatase (ALP) activity of cells interacting with BMP2 within the scaffold. To determine the favorable BMP2 concentration within the BMP2/*hb*-PNCOL, BMP2 dosage of 0, 100, 200, 400, 600 and 800 ng/ml of BMP2was admixed within BMP2/*hb*-PNCOL, and ALP activity of the cells measured after 10 days in culture. For analysis, ALP activity of MC3T3-E1 cells encapsulated in their respective scaffold was measured using our established protocol [31] after ten days of culture in complete media.

2.2.5. Measuring kinetic BMP2 release from injectable scaffold

Upon identifying the components of injectable orthobiologic scaffold, the kinetic BMP2 release profile was measured over 21 days using BMP2 Quantikine enzyme-linked immunosorbent assay (ELISA) (R&D systems). The BMP2/*hb*-PNCOL scaffolds were synthesized and incubated in PBS. The release kinetics of BMP2 from the scaffold was determined by aspirating the supernatant from each sample completely, and replacing it with equivalent volume of fresh PBS at 1, 2, 4, 6, 10, 14, 17 and 21 days. The BMP2 concentrations in the collected samples were determined following the manufacturer's protocol.

2.3. Long-term in vitro performance assessment of the injectable orthobiologic scaffold

To evaluate the long-term *in vitro* osteoinductive potential of injectable orthobiologic scaffolds BMP2/*hb*-PNCOL, 3% (w/v) PCL scaffolds

incorporated with 200 ng/ml BMP2 blended with heparin and BSA in 1:40:2000 ratio were cultured in osteogenic media for 21 days. PNCOL scaffolds without BMP2 was used as a control group. The scaffolds were evaluated in terms of cell proliferation, ALP activity, matrix mineralization, and osteoblast-specific gene expression profiles at days 0, 7, 14, and 21.

2.3.1. Cell proliferation

Cell proliferation within BMP2/*hb*-PNCOL scaffolds was evaluated using the non-toxic alamarBlue® cell viability assay kit (Life Technologies, USA). 0.5 ml of 20% alamarBlue reagent in complete media was added to each sample and incubated for 2 h at 37 °C. The media from each sample was collected and the fluorescence values were measured using a microplate fluorometer (Wallac 1420) at 565 nm excitation and 585 nm emission wavelengths. Total cell number was determined using a standard curve generated with varying number of cells and their corresponding fluorescence values.

2.3.2. Cell differentiation

The cellular *alkaline phosphatase* (*ALP*) *activity* was determined by quantifying the amount of p-nitrophenol (pNP) converted from p-nitrophenyl phosphate (pNPP) substrate (Sigma-Aldrich, USA) in presence of ALP. The samples frozen in liquid nitrogen were mechanically disrupted, resuspended in an alkaline lysis buffer (10 mM Tris–HCl, 2 mM $MgCl_2$, 0.1% Triton X-100, pH 8), and lysed using a homogenizer. The supernatant was mixed with the pNPP substrate at 1:1 ratio and incubated at 37 °C for 30 min. The reaction was stopped using 3 N NaOH and the color developed was quantified using a microplate spectrophotometer (SpectraMax) at 405 nm wavelength. The total ALP was estimated using a standard curve obtained with dilutions of calf alkaline phosphatase enzyme and was normalized with respect to the total protein content in each sample. Total protein content was determined by Coomassie Bradford protein assay kit (Thermo Scientific, USA) following the manufacturer's protocol.

The progression of *matrix mineralization* within the scaffolds was quantified using Alizarin red S solution (Millipore, USA). The frozen samples were mechanically disrupted, incubated in Alizarin red S solution for 20 min and washed 6X with PBS. 10% acetic acid was added to each sample, incubated for 30 min and heated at 85 °C for 10 min to dissolve the calcium deposits. The solution was neutralized with 10% ammonium hydroxide to adjust the pH to 4.3, centrifuged and the supernatant was read at 405 nm wavelength in a microplate spectrophotometer (SpectraMax). The standard curve was generated by using different concentrations of Alizarin red solution and their respective absorbance values.

The *osteoblast-specific gene expression profiles* of BMP2/*hb*-PNCOL and control PNCOL groups were determined by performing real-time polymerase chain reaction (RT-qPCR). The fresh scaffolds were crushed in lysis buffer and total RNA from samples was extracted using the RNeasy mini kit (Qiagen) following the manufacturer's instructions.1 μg of RNA was reverse transcribed to cDNA using the QuantiTect Reverse Transcription Kit (Qiagen) following manufacturer's protocol. Real-time quantitative polymerase chain reaction (qPCR) was performed with SYBR Select PCR master mix (Applied Biosystems, Life Technologies) for ALP, osterix (OSX), osteopontin (OP), and osteocalcin (OCN), with hydroxymethylbilane synthase (HMBS) as the normalizing gene. The primer sequences (Table 1) obtained from published literature [35–39] were verified using OligoAnalyzer and purchased from IDT (Integrated DNA Technologies). PCR amplification was performed in iCycleriQ detection system (Biorad) with thermocycling performed for 10 min at 95 °C followed by 40 cycles at 95 °C for 15 s and 56 °C for 60 s. Expression of each gene was normalized to the gene expression level of the day 0 samples for each condition. Data were analyzed for fold difference in gene expression using the ΔΔCt method.

2.3.3. Visualization of mineralized deposits

The mineralized deposits within the BMP2/*hb*-PNCOL and PNCOL scaffolds were visualized by histological analysis and Von Kossa staining. PNCOL scaffolds at days 7, 14, and 21 were fixed in 10% formalin for 24 h, dehydrated using an ethanol gradient and incubated in xylene before embedding them in paraffin. The embedded samples were sectioned at 20 μm thickness and mounted on microscope slides. The rehydrated sections were incubated in Von Kossa stain, washed and viewed under a bright field microscope to observe the mineralized matrix.

2.4. Statistical analyses

Statistical analysis was performed using Student's t-test and One-way ANOVA. All values are reported as the mean and ± the standard deviation of the mean. $p < 0.05$ was considered to be statistically different.

3. Results

3.1. Synthesis and characterization of injectable nanofibrous cell-embedded orthobiologic biomaterial

The injectable nanofibrous scaffold with pre-osteoblasts and osteogenic factor was manufactured by incorporating electrospun PCL nanofibers within the collagen type-I solution containing pre-osteoblast cells and BMP2 (with and without heparin/BSA). PCL nanofibers were obtained by electrospinning technique and homogenized. Based on our established O_2 plasma functionalization protocols [32,40,41], oxygen containing functional groups were introduced on PCL surface to decrease its hydrophobicity and enhance PCL nanofiber's cell and protein. The functionalized PCL nanofibers were admixed homogenously within the neutralized collagen solution containing BMP2 and cells. The incorporation of PCL nanofiber created major changes in the structural, viscoelastic, and protein retention properties of the scaffold.

3.1.1. The changes in external and internal scaffold morphology

The effect of PCL nanofiber on the injectable scaffold's morphology and porosity was investigated using SEM micrographs and surface area analysis. Fig. 2 demonstrated SEM micrographs of PNCOL scaffolds with various PCL concentrations. The SEM micrographs showed that size of void areas reduced with increased PCL nanofiber concentration within the scaffold. Prior to adding nanofibers within the collagen (0% PNCOL), the scaffold had pore sizes ranging from 10 to 40 μm on the surface. For 6% (w/v) PNCOL, pore sizes dropped to almost 500 nm compared to 0% (w/v) PNCOL (Fig. 2).

Table 1
Forward and reverse primers for real-time PCR.

Gene	Forward primer	Reverse primer	Ref
HMBS	5′ GAGTCTAGATGGCTCAGATAGCATGC 3′	5′ CCTACAGACCAGTTAGCGCACATC 3′	[35]
ALP	5′ GATCTTCTTTCTCCTTTGCCTGG 3′	5′ TGTTTGCAGTGGTGGTTCTGGCA 3′	[36]
OSX	5′ TGGCCATGCTGACTGCAGCC 3′	5′ TGGGTAGGCGTCCCCCATGG 3′	[37]
OP	5′ GGCATTGCCTCCTCCCTC 3′	5′ GCAGGCTGTAAAGCT TCTCC 3′	[38]
OCN	5′ TGCTTGTGACGAGCTATCAG 3′	5′ GAGGACAGGGAGGATCAAGT 3′	[39]

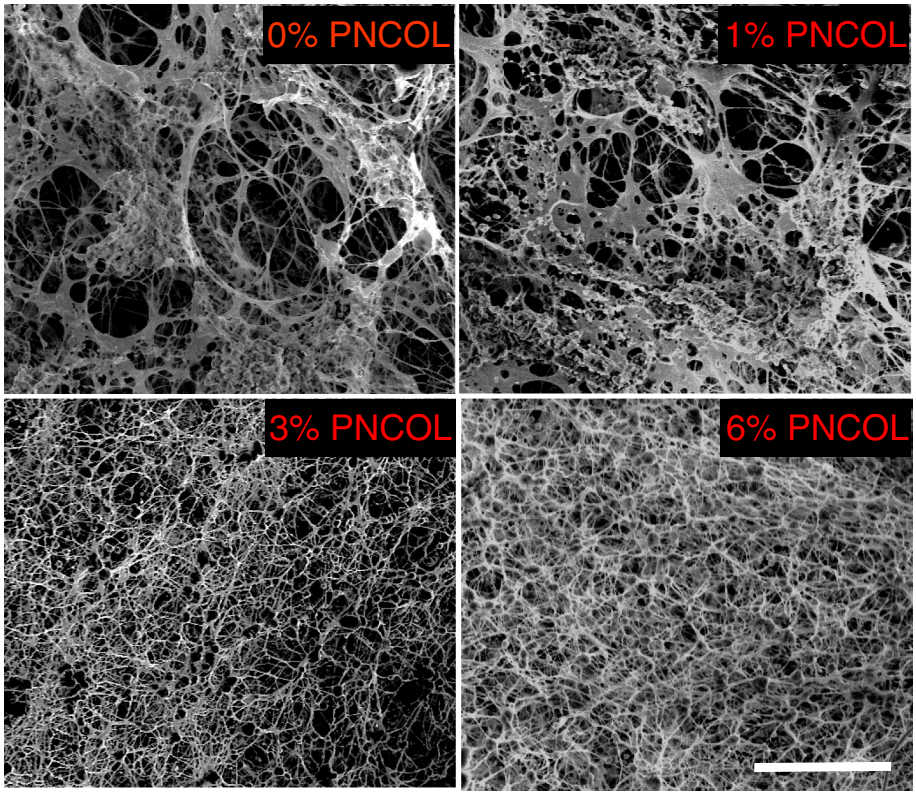

Fig. 2. SEM micrographs of PNCOL scaffolds with various PCL nanofiber concentrations. Increased PCL nanofiber concentrations within the injectable scaffolds reduced the pore sizes on the surface. The scale bar is 40 μm.

3.1.2. The changes in scaffold viscoelastic properties

In rheological analysis, G′ (storage or elastic modulus) describes the solid behavior of the material, while G″ (loss or viscoelastic modulus) describes the liquid behavior of the material. Fig. 3 displays the rheological analysis for G′ and G″ as a function of frequency for PNCOL with various PCL concentrations.

Similar trend was observed in internal scaffold morphology, determined by the changes in total *internal* surface area of the scaffold measured by a surface area and porosimetry analyzer. The results tabulated in Table 2 demonstrate that the internal macroporous surface area decreased with increased PCL concentration within PNCOL. 0% (w/v) PNCOL had the highest surface area with a value of 42.467 m^2/g, while 1%, 3%, and 6% (w/v) PNCOL scaffolds showed around 2-fold, 3.5-fold and 6-fold decrease in the measured total surface area, respectively. These reductions in the surface area were attributed to the decrease in macroporous structure within the scaffold.

Fig. 3A demonstrates that the storage (elastic) modulus increased with increased PCL concentration within the PNCOL. This increment was statistically significant ($p < 0.05$) for 3% and 6% (w/v) PNCOL scaffolds. For 3% (w/v) PNCOL, G′ (storage modulus) increased 200-fold compared to pure collagen and reached to around 1000 Pa. The G′ values around 103 Pa displays the mechanical stability and stiffness of the material, which can be ideal for bone tissue scaffold. For 6% (w/v) PNCOL, G′ values increased 1000-fold compared to pure collagen and

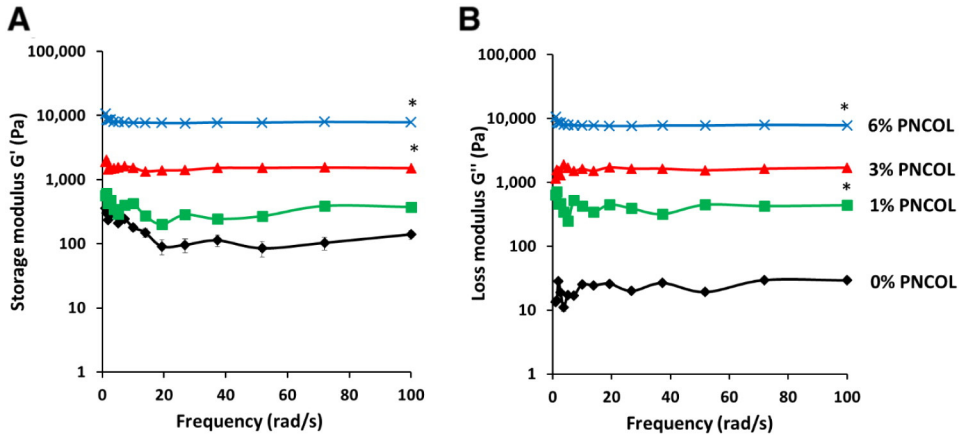

Fig. 3. Rheological analysis for storage (G′) and loss modulus (G″) as a function of frequency for injectable scaffolds with various PCL nanofiber concentrations. Six samples were used for each group (n = 6). (*) indicates significant difference as compared to the adjacent lower concentration of PNCOL $p < 0.05$. Inclusion of PCL provides a remarkable increase in the viscoelastic properties of the scaffold.

Table 2
The changes in the mass, average density, and macroporous surface area of injectable scaffolds with increased PCL nanofiber concentrations.

Scaffolds	Mass[a] (g)	Average density[b] (g/l)	BET macroporous internal surface area[b] (m^2/g)
0% PNCOL	0.0081	40.5	42.4669
1% PNCOL	0.0171	85.5	23.4416
3% PNCOL	0.0320	160.0	12.6449
6% PNCOL	0.0543	271.5	7.6039

[a] Data obtained following freeze drying process.
[b] Data obtained from N_2 adsorption isotherms using BET analysis.

reached to around 10,000 Pa. Overall, storage (elastic) modulus data indicated that PNCOL scaffold become mechanically stable with the increased PCL concentration.

Fig. 3B demonstrates that there was a significant increase in the loss (viscoelastic) modulus with increased PCL concentrations within the scaffold. For 0% (w/v) PNCOL, the viscoelastic modulus was around 10 Pa, which indicated that 0% (w/v) PNCOL (pure collagen) demonstrated more liquid behavior than gel behavior. This fact was changed with the incorporation of PCL with the collagen. The loss (viscoelastic) modulus was increased 100-fold for 1% (w/v) PNCOL and 3% (w/v) PNCOL, and 1000-fold for 6% (w/v) PNCOL compared to 0% (w/v) PNCOL. In sum, loss (viscoelastic) modulus data showed that inclusion of PCL nanofibers within collagen matrix significantly enhanced the injectable scaffold's viscoelastic properties.

3.1.3. Protein retention and protein bioactivity within injectable orthobiologic scaffold

To investigate whether PCL nanofiber incorporation within the scaffold has a role in preventing protein burst release and increasing the protein retention, long-term (21-days) and short-term (4-hours) protein release were conducted. Fig. 4 displays the results of model protein retention and bioactivity of BMP2 within the injectable PNCOL scaffolds.

Protein retention capacity of the scaffold was evaluated using the model protein lysozyme. Fig. 4A demonstrated the short-term protein retention data, which demonstrated that 6% (w/v) PNCOL had the highest protein retention rate compared to the remaining groups. During 4 h, 20 ± 1.28% of initially loaded protein was released for 6% (w/v) PNCOL scaffold, while this percentage was 60 ± 2.18% for 0% (w/v) PNCOL. Fig. 4B displays the long-term (21 days) protein release data from injectable PNCOL scaffolds with various PCL concentrations. The long-term protein release study established that increased PCL nanofiber concentration within the scaffold enhanced the protein retention capacity of injectable scaffold. Over 21 days, 3% (w/v) PNCOL and 6% (w/v) PNCOL retained 62 ± 0.79% and 78 ± 0.98% of the protein within the scaffold respectively, while all protein within 0% PNCOL (collagen) was leached out within 2 days (Fig. 4B). Overall, protein retention results demonstrated diminished burst release and enhanced protein retention with increased PCL concentration within the scaffold.

Fig. 4C shows the bioactivity of BMP2 within PNCOL scaffolds with various PCL concentrations. The protein bioactivity was assessed by

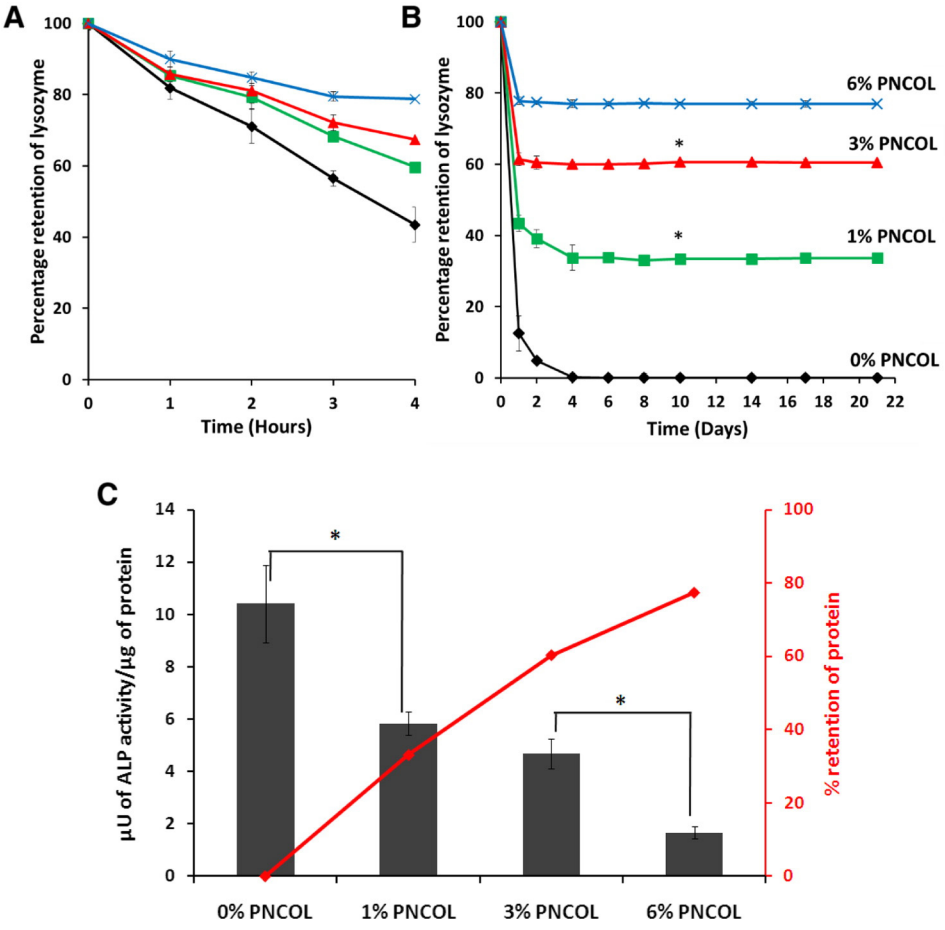

Fig. 4. The role PCL nanofiber concentrations in model protein retention and bioactivity of BMP2 within the injectable PNCOL scaffolds. (A) Lysozyme retention profile within PNCOL scaffolds (n = 4) incorporated with 0, 1, 3, and 6% (w/v) PCL nanofibers during time = 0 to 4 h corresponding to the burst release phase and (B) over 21 days. Protein retention data demonstrated a significant increase with incorporation of PCL nanofibers. (C) Bioactivity of BMP2 within the scaffolds measured in terms of ALP activity of cells encapsulated in PNCOL (n = 4) after ten days in culture is shown in the column graph. The red line graph indicates the percentage of protein (lysozyme) retained in the respective PNCOL scaffolds at day 10. Together, incorporation of PCL nanofibers shows an increase in protein retention but a decrease in protein activity. (*) indicates significant differences compared to the adjacent lower concentration of PNCOL $p < 0.05$. (For interpretation of the references to color in this figure legend, the reader is referred to the web version of this article.)

measuring the ability of BMP2 to increase cellular ALP enzyme synthesis within the scaffold during ten days of culture. Fig. 4C demonstrates that ALP activity, which correlates to the BMP2 activity within the scaffold, decreased with inclusion of PCL nanofibers. Though inclusion of PCL resulted in higher protein retention capacity, it had an adverse effect on the BMP2 bioactivity within the scaffold. 1% and 3% (w/v) PNCOL demonstrated 38 ± 0.48% protein retention and 62 ± 0.58% with 2-fold loss of BMP2 activity ($p < 0.05$) when compared to 0% PNCOL (pure collagen). 6% (w/v) PNCOL provided 78 ± 0.48% protein retention, but had over 5-fold loss of BMP2 activity ($p < 0.05$). Overall, there was a reverse correlation between the scaffold's protein retention capacity and preserving protein bioactivity. Based on above findings, 3% (w/v) PNCOL scaffold was found to possess the desired properties to be employed as an injectable osteoinductive scaffold, with a favorable balance between mechanical, protein retention, and biological properties. Thus 3% (w/v) PNCOL scaffold was chosen for all subsequent studies with BMP2 and for long-term *in vitro* study.

3.1.4. Preserving BMP2 bioactivity within injectable orthobiologic scaffold

There was 2-fold loss in protein bioactivity for 3% (w/v) PNCOL. Thus, preserving BMP2 bioactivity within 3% (w/v) PNCOL was essential prior to conducting *in vitro* study. To achieve that, BMP2 was admixed with heparin and/or bovine serum albumin (BSA) before incorporating within the PNCOL scaffolds. The bioactivity of BMP2 within each group was estimated by measuring the ALP activity of the cells encapsulated in the scaffolds after ten days in culture. Fig. 5A shows the changes in ALP activity with PNCOL scaffolds with heparin and/or BSA. Fig. 5A suggests that the BMP2 activity was protected best in the presence of *both* heparin and BSA, with over a 2-fold increase in ALP activity compared to BMP2-PNCOL (control group) ($p < 0.05$). The result from BMP2/*h*-PNCOL indicated that the solo effect of heparin in bioactivity preservation was not statistically different from control group. On the other hand, BMP2/*b*-PNCOL demonstrated 1.5-fold higher ALP activity compared to control group ($p < 0.05$),which indicated that BSA played a dominant role in preserving the bioactivity of protein encapsulated within the orthobiologic material in comparison to heparin. However, for maximum protein bioactivity preservation, BSA and heparin needed to be utilized together and hence, BMP2/*hb*-PNCOL scaffold was used in subsequent studies.

To determine the favorable BMP2 concentration within BMP2/*hb*-PNCOL, BMP2 dosages ranging from 0 ng/ml to 800 ng/ml was admixed within BMP2/*hb*-PNCOL, and ALP activity of the cells was measured after 10 days in culture (Fig. 5B). Fig. 5B demonstrated that the ALP activity was increased 3.5-fold and 4.5-fold for 100 ng/ml and 200 ng/ml BMP2 concentrations compared to 0 ng/ml BMP2 (control), respectively. There was no statistical difference between the ALP activity of cells with 200, 400, and 600 ng/ml BMP2 concentrations. At a dose of 800 ng/ml, the ALP activity was significantly decreased with respect to the activity at 200 ng/ml dosage, although there was still 2.5 fold increase compared to control. The BMP2 dosage study demonstrated that there was an optimal BMP2 concentration to be incorporated within an injectable BMP2/*hb*-PNCOL with a range between 200 ng/ml and 600 ng/ml. Hence, 200 ng/ml concentration of BMP2 was chosen for future studies.

The kinetic release of BMP2 from BMP2/*hb*-PNCOL scaffold was quantified using ELISA as shown in Fig. 5C. 40 ng of BMP2 was

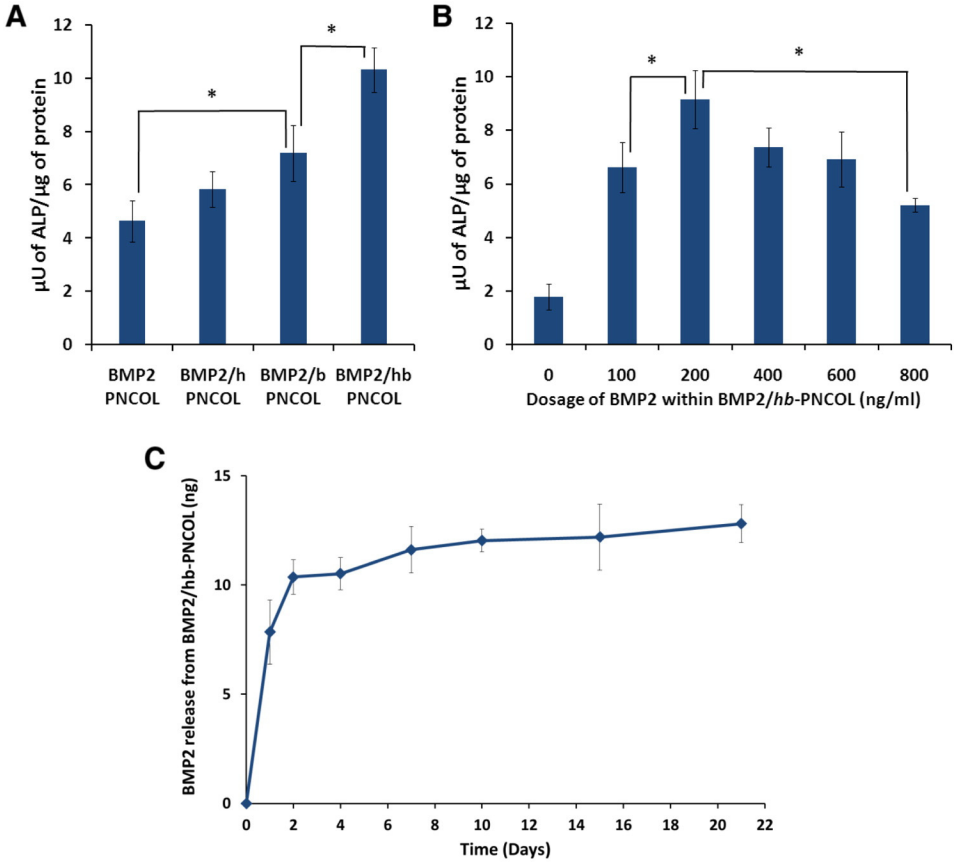

Fig. 5. The role of heparin/BSA and the BMP2 dosage within the injectable scaffold on ALP activities of encapsulated MC3T3-E1 cells and the kinetic release profile of BMP2 from BMP2/*hb*-PNCOL over 21 days. (A) Solo and combined effect of heparin and BSA on preserving and enhancing the bioactivity of BMP2 within 3% (w/v) PNCOL scaffolds ($n = 4$) evaluated by cellular ALP activity after ten days in culture. BMP2 in presence of both heparin and BSA shows highest ALP activity within scaffold. (B) Effect of BMP2 dosage on cellular ALP activity within BMP2/*hb*-PNCOL scaffolds ($n = 4$) determined after ten days in culture. 200 ng/ml BMP2 exhibits highest ALP activity within scaffolds. (*) indicates significant difference in comparison to indicated group at the same time point $p < 0.05$. (C) Amount of BMP2 released from BMP2/*hb*-PNCOL scaffolds ($n = 4$) over 21 days estimated through ELISA.

initially loaded into the scaffold and the release was monitored over 21 days. In the first day, 7.84 ± 2.5 ng BMP2 released from the 40 ng BMP-2 loaded BMP2/*hb*-PNCOL scaffold. Starting from day 2, BMP2 had a sustained release profile with 12.2 ± 3 ng released amount over the 21 days. The BMP2 release study confirmed that there is a gradual and controlled release of BMP2 from BMP2/*hb*-PNCOL over a 21-day period.

3.2. Long-term in vitro performance of injectable osteoinductive BMP2/hb-PNCOL scaffold

The *in vitro* performance of injectable BMP2/*hb*-PNCOL scaffolds was evaluated for 21 days through investigating the proliferation and differentiation of MC3T3-E1 residing within the BMP2/*hb*-PNCOL.PNCOL without BMP2 was used as the control group and both scaffold groups were cultured in osteogenic media.

3.2.1. Cell proliferation

Cell proliferation of MC3T3-E1 within BMP2/*hb*-PNCOL and PNCOL were measured for 21 days using alamarBlue assay. The cell proliferation data (Fig. 6A) demonstrated that there was a sharp increase in cell numbers from in the first 7 days and the cells continued proliferating until day 14 within both BMP2/*hb*-PNCOL and control scaffolds. At day 14 and day 21, there was no statistical difference between the cell numbers for BMP2/*hb*-PNCOL and control group ($p > 0.05$). A dramatic decrease in the rate of proliferation is seen after day 14 within both scaffold groups due to onset of differentiation into osteoblasts, which was confirmed with ALP activity measurements over 21 days. The data indicates that BMP2/*hb*-PNCOL and PNCOL scaffolds allowed the proliferation of MC3T3-E1 cells within their structure.

3.2.2. Cell differentiation

The differentiation of MC3T3-E1 cells within the BMP2/*hb*-PNCOL and PNCOL scaffolds was evaluated by measuring the ALP activity, matrix mineralization, and osteoblast-specific gene expression profile for 21 days.

The *ALP activity* of MC3T3-E1 cells was measured using pNPP alkaline phosphatase substrate and normalized with total protein. As shown in Fig. 6B, the ALP activity increased sharply throughout the 21 days within BMP2/*hb*-PNCOL, while there is no statistically different increase in ALP activity after day 14 in case of the control scaffolds. Furthermore, at day 14 and day 21, cells within BMP2/*hb*-PNCOL had higher ALP activity compared to those within the control group ($p < 0.05$). *Matrix mineralization* within BMP2/*hb*-PNCOL and PNCOL (control) scaffolds was quantified for over 21 days using Alizarin red S solution and normalized with total protein. As shown in Fig. 6C, the mineralization data revealed to be consistent with the results of ALP activity. The results demonstrate that there was no substantial mineralization for the first seven days for both groups. There was an increase in mineralization at day 14 for BMP2/*hb*-PNCOL group when compared to day 7 ($p < 0.05$). On the other hand, there was no mineralization within PNCOL (control) scaffolds for the first 14 days. At day 21, the amount of mineralization in BMP2/*hb*-PNCOL scaffolds was significantly higher than the scaffolds without BMP2 ($p < 0.05$). This indicates that BMP2 within the BMP2/*hb*-PNCOL maintained its activity over 21 days and plays a role in accelerating osteogenesis and enhancing mineralization. The ALP activity and matrix mineralization data together demonstrate that BMP2/*hb*-PNCOL scaffolds not only promote cell proliferation within the scaffold but also provide an osteoinductive environment for osteoblastic differentiation over 21 days.

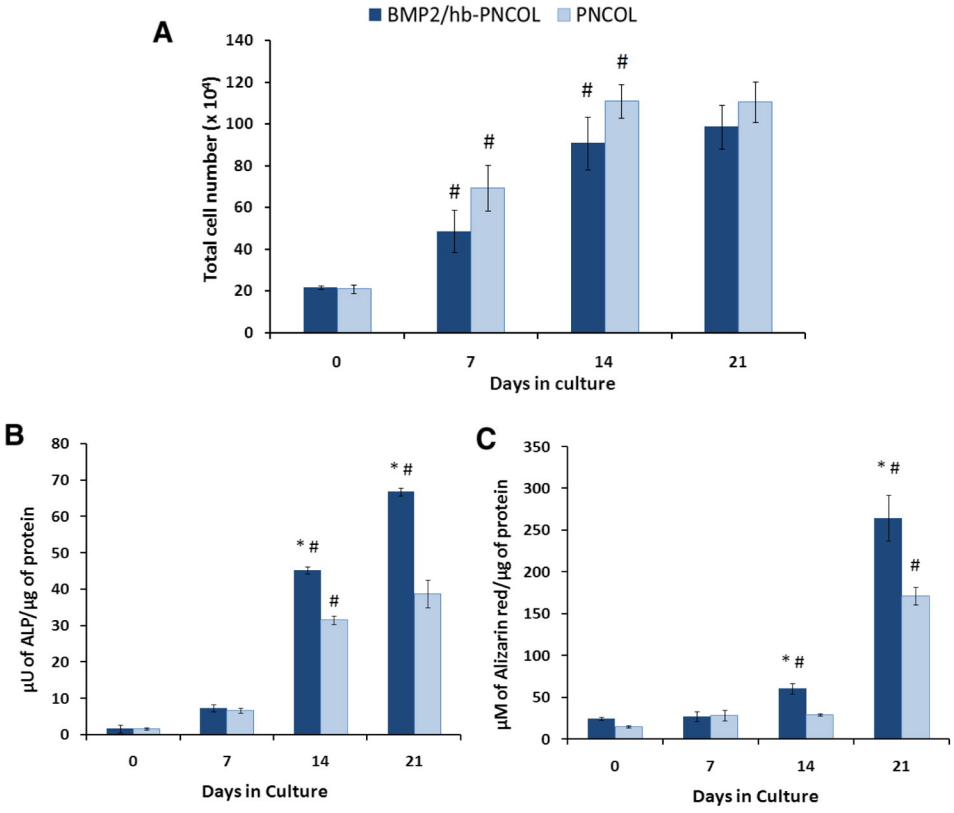

Fig. 6. Long term *in vitro* evaluation of BMP2/*hb*-PNCOL scaffolds. (A) Cell proliferation, (B) alkaline phosphatase activity, and (C) Alizarin red quantification of mineralized deposits within BMP2/*hb*-PNCOL and PNCOL scaffolds ($n = 4$) cultured in osteogenic media from day 0 to day 21. Cells proliferate within the scaffolds until day 14 and thereafter maintained through day 21 with no statistical difference between the two groups. Both ALP activity and mineralized matrix quantification normalized against total protein of the respective BMP2/*hb*-PNCOL scaffolds exhibits significant increases at days 14 and 21 as compared to PNCOL scaffolds (control). (*) indicates significant difference in comparison to PNCOL (control group) at the same time point. (#) indicates significant differences as compared to earlier time points of the same group $p < 0.05$. The results demonstrate the osteoinductive potential of BMP2/*hb*-PNCOL scaffolds.

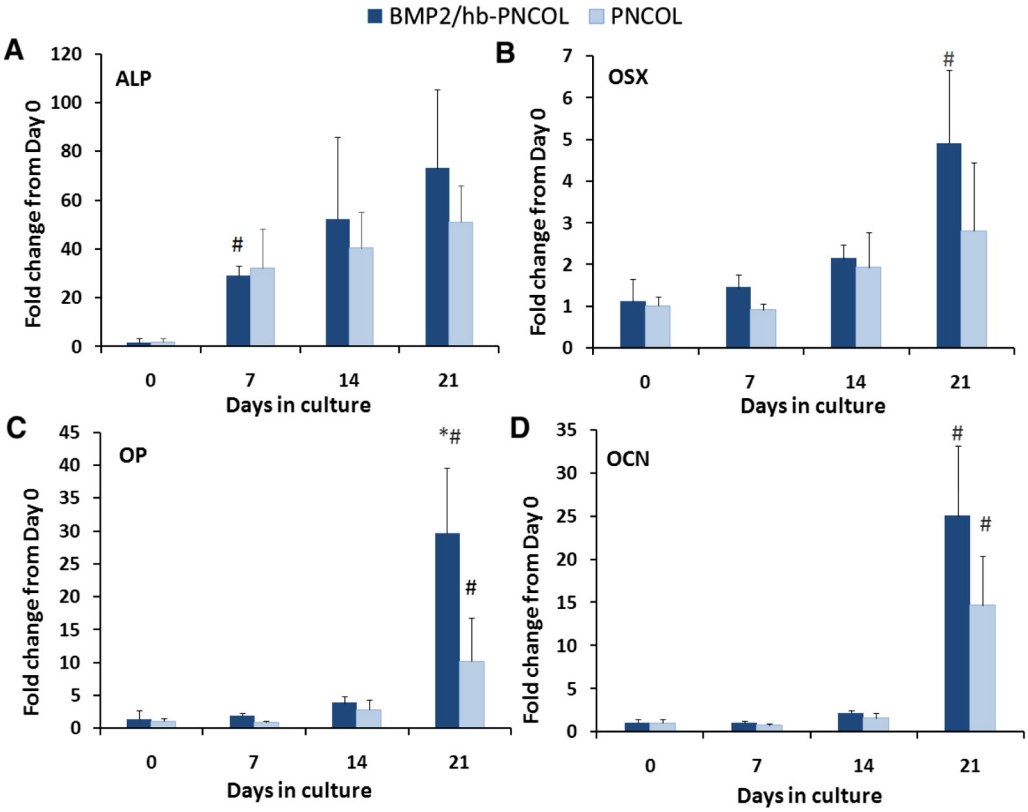

Fig. 7. Osteoblast-specific gene expression profile over 21 days. Expression of early- and late-osteoblastic differentiation markers (A) alkaline phosphatase (B) osterix (OSX) (C) osteopontin (OP) (D) osteocalcin (OCN) within BMP2/*hb*-PNCOL and PNCOL (control) scaffolds (n = 4) cultured in osteogenic media from day 0 to day 21 evaluated using RT-qPCR. The gene expression profiles shows increases over 21 days (*) indicates significant difference in comparison to control scaffolds at the same time point. (#) indicates significant differences as compared to earlier time points of the same group $p < 0.05$.

Fig. 7 shows expression levels of early and late osteoblast-specific genes, namely ALP, osterix, osteopontin, and osteocalcin over 21 days obtained using RT-qPCR.

The gene expression data was presented as fold change in expression of each gene with respect to its expression level at day 0. As seen in Fig. 7A, a continuous increase in fold change of ALP expression was observed within BMP2/*hb*-PNCOL and PNCOL scaffolds over 21 days. Though the average ALP expression was higher in BMP2/*hb*-PNCOL when compared to the control group at day 14 and day 21, they were not statistically different. As demonstrated in Fig. 7B, expression of osterix at day 0 was unchanged until day 14; however at day-21, there was a 50% increase in fold change for BMP2/*hb*-PNCOL group, while only a small (not statistically significant) increase was seen in the control scaffolds. Gene expression profiles of late differentiation markers osteopontin and osteocalcin were similar to each other. During the first 14 days, there was no significant change in both osteopontin and osteocalcin expression for BMP2/*hb*-PNCOL and PNCOL scaffolds. However, at day 21, there was a steep jump in osteopontin expression

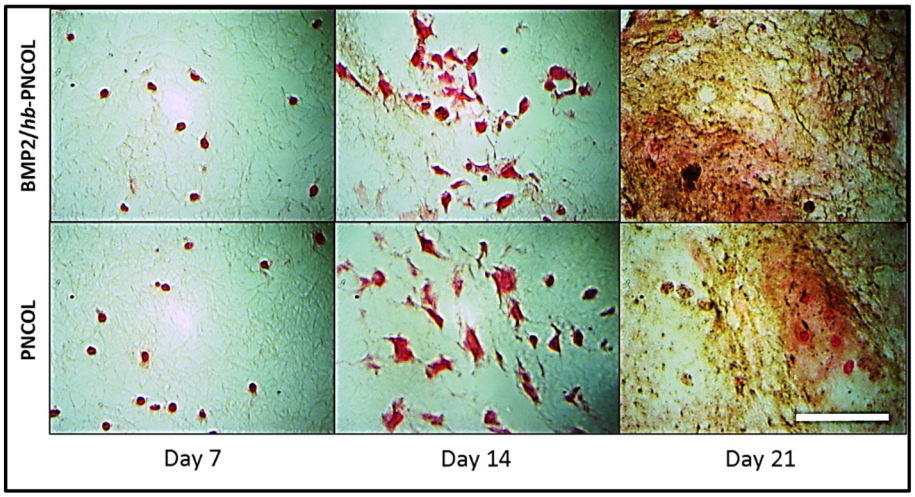

Fig. 8. Histology sections of BMP2/*hb*-PNCOL and PNCOL scaffolds cultured in osteogenic media on days 7, 14, and 21. Von Kossa staining indicates the mineralized matrix deposition within the scaffold. Mineralized deposits are represented by brown color, and cells are stained red. Scale bar represents 100 μm. (For interpretation of the references to color in this figure legend, the reader is referred to the web version of this article.)

with over a 650% increase for BMP2/*hb*-PNCOL scaffolds and roughly a 250% increase for PNCOL scaffolds. Meanwhile, osteocalcin expression showed over 710% increase for BMP2/*hb*-PNCOL and around 500% increase for PNCOL scaffolds. Taken together, the osteoblast-specific gene expression results demonstrated that the injectable BMP2/*hb*-PNCOL scaffold is osteoinductive and promotes the gene expression of osteoblastic differentiation markers over 21 days.

3.2.3. Visualization of mineralized deposits

The progression of mineralization within the scaffolds was visualized through Von Kossa staining of histology sections. Fig. 8 shows representative images of the extent of mineralized matrix deposition within BMP2/*hb*-PNCOL and PNCOL scaffolds at days 7, 14 and 21. It is observed that there are no mineralized deposits at day 7, while a slight indication of mineralization is noticed at day 14. On day 21, the histology slides show a dramatic increase in the mineralized matrix secretion, confirming that the cells were terminally differentiated and functional within the scaffold. The BMP2/*hb*-PNCOL scaffold slide had more mineralized matrix than PNCOL scaffold slide. This indicates that BMP2 within the BMP2/*hb*-PNCOL scaffold plays a role in accelerating the osteogenic differentiation of osteoprogenitor cells.

4. Discussion

There is a great need for injectable osteoinductive biomaterials with proper biological, mechanical, and structural properties that ensure sustained release of growth factors without loss of protein activity for bone regeneration at the defect site. Our objective in this study was to employ a mechanistic approach in synthesizing an injectable orthobiologic scaffold encapsulated with pre-osteoblasts and BMP2 that is capable of increasing the protein retention while maintaining its bioactivity, and creating an osteoinductive microenvironment for terminal differentiation into osteoblasts. To achieve this goal, we have created a nanofibrous injectable bone filler BMP2/*hb*-PNCOL, which combines the superior mechanical properties of electrospun PCL nanofibers with the excellent biological properties of collagen type-I to form a structurally stable scaffold that can accommodate both cells and growth factor within its intricate three-dimensional structure. Our data demonstrated that the PCL nanofibers within the injectable material dictated the protein retention, viscoelastic properties, and external and internal morphology of the composite scaffold. Incorporation of biomolecules heparin and BSA maintained the bioactivity of the encapsulated BMP2. Controlled release of BMP2 was achieved for 3 weeks without loss of bioactivity and the encapsulated osteoprogenitor cells expressed osteoblast-specific genes and terminally differentiated over a 21-day period.

Incorporation of PCL nanofiber within collagen played a major role in altering the injectable scaffold's external and internal structure along with its viscoelastic properties. The SEM micrographs (Fig. 2) and surface area analysis (Table 2) demonstrated that the macroporosity of the scaffold decreased with addition of PCL nanofibers within PNCOL and created a denser network of collagen-PCL fibers. The external and internal macroporous structure was replaced by a more nanoporous structure on increasing the PCL nanofiber concentration within the injectable material. This increase in nanofibrous structure of the scaffold with the inclusion of PCL dramatically in turn enhanced the viscosity and elasticity of the composite scaffold (Fig. 3), making it structurally stable and mechanically robust.

The influence of PCL nanofiber incorporation within collagen was most remarkable in terms of the protein release profile, with increased PCL nanofiber concentration exhibiting a higher rate of protein retention within the scaffold. The superior protein retention capacity of PNCOL scaffolds can be associated with the nanofibrous internal structure of the scaffold as well as the functional groups present on the surface of PCL nanofibers. For 3% (w/v) PNCOL and 6% (w/v) PNCOL retained 62 ± 0.79% and 78 ± 0.98% of the protein within the scaffold, respectively. Pure collagen scaffolds, on the other hand, released the entire loaded protein within 2 days in culture due to their highly macroporous structure. Secondly, carboxyl and hydroxyl functional groups introduced on PCL surface through O_2-plasma treatment [32,40,41] can create binding between BMP2 and PCL nanofibers, which can prevent burst release (Fig. 4A) and can retain BMP2 within the injectable matrix (Fig. 4B). These oxygen-containing functional groups are electron donors and hence increase the negative charge on the polymer surface [42]. BMP2, on the other hand, is a positively charged protein with a free-end amine group in an aqueous solution [43,44]. Thus, there is a strong electrostatic attraction between positively charged BMP2 and negatively charged PCL nanofiber along with the covalent binding between the primary amine groups ($-NH_2$) of BMP2 and the various oxygen-rich functional groups on plasma-treated PCL nanofibers. Incorporating O_2-plasma modified PCL nanofibers within collagen can hence help retaining the protein within the injectable composite scaffold for the duration required to achieve osteogenesis and matrix mineralization (Fig. 6C).

Even though increased PCL nanofiber concentration within the PNCOL scaffold provided higher protein retention, it also adversely affected the bioactivity of BMP2 encapsulated within the scaffold. A significant loss of protein activity was observed at higher concentrations of PCL within the scaffold (Fig. 4C). This result could be attributed to the increased shear forces applied through pipetting during PNCOL synthesis. With the increased PCL concentration, specifically for 3% (w/v) and 6% (w/v) PNCOL synthesis, a vigorous pipetting had to be applied to the collagen-PCL nanofiber solution to distribute PCL nanofibers homogenously within the collagen. The shear force exerted on the encapsulated protein could have possibly damaged the protein structure and reduced its bioactivity. Thus, a systematic and deliberate study was conducted to create a cell- and protein embedded, yet mechanically robust, injectable orthobiologic scaffold. The mechanical, structural, and biological properties of this composite scaffold could be tuned by varying the PCL nanofiber concentration within the scaffold. For instance, 6% (w/v) PNCOL, though had higher protein retention, saw over a 80% reduction in protein activity, while 1% (w/v) PNCOL had poor protein retention along with 50% loss in bioactivity of encapsulated protein (Fig. 4C). Hence the results shown in Figs. 2, 3, and 4 demonstrated that 3% (w/v) PNCOL was the most viable configuration to create the BMP2-incorporated injectable scaffolds because of its 20-fold higher viscoelastic properties compared to pure collagen, ability to retain 62% of protein within the scaffold over 21 days with only 50% loss in bioactivity.

The bioactivity of BMP2 within 3% (w/v) PNCOL was restored by introducing heparin and bovine serum albumin (BSA) around the protein. In this study, we have identified the solo and combinatorial effect of heparin and BSA on BMP2 bioactivity preservation (Fig. 5A). Our results revealed that heparin and BSA, together, constituting the BMP2/*hb*-PNCOL scaffold, significantly minimized the loss of protein bioactivity. This result (Fig. 5A) can be attributed to the unique properties of heparin and BSA, which play different roles in preserving BMP2 bioactivity. BSA, widely used as a protective agent for growth factors is likely to provide a layer around BMP2 and shield the protein against possible residual organic solvents left on the PCL nanofibers [17,27]. BSA also could protect BMP2 from possible structural damage due to shear forces exerted on protein during incorporating PCL nanofibers within the collagen through pipetting. Heparin, on the other hand, is known to bind to BMP2 directly through electrostatic interactions between N-/O-sulfated residues of heparin and the lysine/arginine residues of BMP2. This electrostatic interaction helps in retaining protein bioactivity by (*i*) prolonging its half-life, (*ii*) decreasing BMP2 localization to other possible bindings, and (*iii*) minimizing inhibitory effect of BMP2 antagonist noggin [30,45]. Thus, we have used heparin and BSA together to create BMP2-incorporated injectable nanofibrous scaffold, BMP2/*hb*-PNCOL, with high protein retention and protein bioactivity preservation capacities. It should be also noted that,

to the best of our knowledge, in this study, heparin and BSA were utilized together for the first time within a scaffold to preserve the protein bioactivity. Furthermore, a low dose of 200 ng/ml BMP2 in presence of heparin and BSA was sufficient to initiate *in vitro* osteoblastic differentiation within the osteoinductive scaffold, and controlled release of BMP2 from BMP2/*hb*-PNCOL scaffold was confirmed as 12.2 ± 3 ng of BMP2 was released over 21 days (Fig. 5B and C).

The *in vitro* performance of these injectable BMP2/*hb*-PNCOL scaffolds was evaluated at days 0, 7, 14, and 21 by measuring the proliferation, differentiation, mineralization, and osteoblast-specific gene expression profile of MC3T3-E1 residing within the scaffolds. PNCOL (without BMP2) was used as a control group for each characterization. Cell proliferation of MC3T3-E1 within BMP2/*hb*-PNCOL and PNCOL scaffolds showed that there was a steady increase in cell number in first 14 days, after which there was a decline in the rate of proliferation (Fig. 6A). These results can be attributed to the starting of terminal differentiation of pre-osteoblast cells to osteoblast, which is accompanied by slower rate of proliferation. In fact, initiation of differentiation was confirmed with ALP activity (Fig. 6B) and ALP gene expression (Fig. 7A). Fig. 6B demonstrated that ALP activity started increasing at day-14, which was an indicator of osteoblastic differentiation. Since ALP is an early differentiation marker for osteoblastic cell, its activity starts to pick up once proliferation reduces and osteoblastic differentiation starts [46]. Also, the ALP activity data (Fig. 6B) demonstrated that cells within the BMP2/*hb*-PNCOL scaffold had the higher ALP activity compared to the cells within PNCOL scaffold. This result can be explained by the BMP2 presence within the matrix and the preserved BMP2 bioactivity. From ALP activity of BMP2-incorporated PNCOL scaffolds (Fig. 4C), we know that mere presence of BMP2 within the scaffold does not guarantee high ALP activity, since there can be loss of bioactivity. Thus, the higher ALP activity exhibited by cells within BMP2/*hb*-PNCOL scaffold also proves that BMP2 activity within the scaffold is preserved over 21 days with the help of heparin and BSA. Heparin and BSA prevent premature degradation of BMP2 and is likely to provide a cushion-like environment, which could have helped preserving BMP2 activity during the scaffold synthesis.

The mineralization data (Figs. 6C and 8) revealed to be consistent with the trend in ALP activity. At day 21, the amount of mineralization quantified by Alizarin red (Fig. 6C) in BMP2/hb-PNCOL scaffolds was significantly higher than control group ($p < 0.05$), while the histology sections (Fig. 8) also show more regions stained for mineralized deposits in BMP2/hb-PNCOL when compared to the control scaffolds. This indicates that BMP2 within the BMP2/hb-PNCOL maintained its activity over 21 days and plays a role in accelerating osteogenesis and enhancing mineralization. The gene expression data (Fig. 7) obtained through RT-PCR demonstrated that in specific, the late osteoblast-specific markers namely osteopontin, and osteocalcin that coincide with the onset of mineralization [47],had highest expression with 650%, and 710% fold change respectively within BMP2/*hb*-PNCOL scaffold over 21 days (Fig. 7C and D). The MC3T3-E1 cells within BMP2/*hb*-PNCOL scaffolds show accelerated differentiation and higher osteogenic differentiation markers at each time point, which demonstrated that not only was BMP2 successfully retained in the scaffold, but its activity also was maintained over 21 days. Overall, the cell proliferation, ALP activity, matrix mineralization, and osteoblast-specific gene expression data demonstrated that that BMP2/*hb*-PNCOL scaffolds promote both cell proliferation within the scaffold and provide an osteoinductive environment for osteoblastic differentiation over 21 days.

This injectable composite scaffold is an innovative technique to accommodate growth factors and cells in a biomaterial, which is biocompatible, possesses acceptable mechanical properties, and able to retain protein for a prolonged period of time while maintaining its activity at the injected site for bone repair and regeneration. The advantage of our composite biomaterial is that it can be tailored by varying the amount of PCL nanofibers in the collagen matrix, to achieve an optimum balance between protein retention and preservation of bioactivity. Through low dosage of BMP2 of 200 ng/ml, this scaffold is able to accelerate and enhance osteoblastic differentiation in presence of osteogenic factors over long-term *in vitro* culture. Since the necessity for high dosage amounts of BMP2 to achieve bone healing [15–17] is one of the major challenges faced in clinical research, this observation is particularly significant. The scaffold though has superior mechanical properties as compared to other injectable gel-based biomaterials, might not be enough to match the mechanical properties of *in vivo* bone. The onset of mineralization within the scaffold, however, would contribute to enhancing the compressive strength of the scaffold, as demonstrated in our earlier work [31].

5. Conclusion

In this study, we have conducted a mechanistic study to establish a novel injectable orthobiologic scaffold system with tunable physical, mechanical, protein retention, and osteoinductive properties. This injectable scaffold system is built through incorporating PCL nanofibers within collagen, along with osteoprogenitor cells, and BMP2 with heparin/BSA. Through changing PCL nanofiber concentration with the system, we were able to enhance the protein retention capacity. Controlled release of BMP2 was achieved for 3 weeks without loss of its bioactivity. The encapsulated osteoprogenitor cells expressed osteogenic differentiation markers and osteoblast-specific gene expression. This study has built the foundation and framework for a versatile injectable material system with synthetic electrospun nanofibers. The biomimetic osteoinductive material is unique because solid-state synthetic nanofibers with very well-known advantages was converted into a semi-solid injectable form. This in turn results in great advantages over the currently used synthetic polymer-collagen materials in terms of injectability, three-dimensionality for cells and protein accommodation within the nanofibrous material.

Acknowledgments

The authors would like to thank Dr. Saleh Jabarin from the Polymer Institute at the University of Toledo for the access to the parallel plate rheometer. This work is supported by the deArce-Koch Memorial Endowment Fund in Support of Medical Research and Development.

Appendix A. Supplementary data

Supplementary data to this article can be found online at http://dx.doi.org/10.1016/j.msec.2015.02.030.

References

[1] A. Brydone, D. Meek, S. Maclaine, Bone grafting, orthopaedic biomaterials, and the clinical need for bone engineering, Proc. Inst. Mech. Eng. H J. Eng. Med. 224 (2010) 1329–1343. http://dx.doi.org/10.1243/09544119JEIM770.
[2] B.R. Constantz, I.C. Ison, M.T. Fulmer, R.D. Poser, S.T. Smith, M. VanWagoner, et al., Skeletal repair by in situ formation of the mineral phase of bone, Science 267 (1995) 1796–1799. http://dx.doi.org/10.1126/science.7892603.
[3] H. Petite, V. Viateau, W. Bensaid, A. Meunier, C. de Pollak, M. Bourguignon, et al., Tissue-engineered bone regeneration, Nat. Biotechnol. 18 (2000) 959–963. http://dx.doi.org/10.1038/79449.
[4] Y. Huang, C. Simmons, D. Kaigler, K. Rice, D. Mooney, Bone regeneration in a rat cranial defect with delivery of PEI-condensed plasmid DNA encoding for bone morphogenetic protein-4 (BMP-4), Gene Ther. 12 (2005) 418–426. http://dx.doi.org/10.1038/sj.gt.3302439.
[5] U. Berlemann, S. Ferguson, L.-P. Nolte, P. Heini, Adjacent vertebral failure after vertebroplasty. A biomechanical investigation, J. Bone Joint Surg. Br. Vol. 84 (2002) 748–752. http://dx.doi.org/10.1302/0301-620X.84B5.11841.
[6] K.-S. Ryu, J.-H. Shim, H.-Y. Heo, C.-K. Park, Therapeutic efficacy of injectable calcium phosphate cement in osteoporotic vertebral compression fractures: prospective nonrandomized controlled study at 6-month follow-up, World Neurosurg. 73 (2010) 408–411. http://dx.doi.org/10.1016/j.wneu.2010.01.006.
[7] A.A. Amini, L.S. Nair, Injectable hydrogels for bone and cartilage repair, Biomed. Mater. 7 (2012) 024105. http://dx.doi.org/10.1088/1748-6041/7/2/024105.
[8] D. Chen, M. Zhao, G.R. Mundy, Bone morphogenetic proteins, Growth Factors 22 (2004) 233–241. http://dx.doi.org/10.1016/B0-12-341103-3/00036-X.

[9] E.A. Wang, V. Rosen, J.S. D'Alessandro, M. Bauduy, P. Cordes, T. Harada, et al., Recombinant human bone morphogenetic protein induces bone formation, Proc. Natl. Acad. Sci. 87 (1990) 2220–2224.
[10] N. Aebli, H. Stich, P. Schawalder, J.C. Theis, J. Krebs, Effects of bone morphogenetic protein-2 and hyaluronic acid on the osseointegration of hydroxyapatite-coated implants: an experimental study in sheep, J. Biomed. Mater. Res. A 73 (2005) 295–302. http://dx.doi.org/10.1002/jbm.a.30299.
[11] L. Meinel, S. Hofmann, O. Betz, R. Fajardo, H.P. Merkle, R. Langer, et al., Osteogenesis by human mesenchymal stem cells cultured on silk biomaterials: comparison of adenovirus mediated gene transfer and protein delivery of BMP-2, Biomaterials 27 (2006) 4993–5002. http://dx.doi.org/10.1016/j.biomaterials.2006.05.021.
[12] T. Katagiri, A. Yamaguchi, M. Komaki, E. Abe, N. Takahashi, T. Ikeda, et al., Bone morphogenetic protein-2 converts the differentiation pathway of C2C12 myoblasts into the osteoblast lineage, J. Cell Biol. 127 (1994) 1755–1766. http://dx.doi.org/10.1083/jcb.127.6.1755.
[13] Y. Takuwa, C. Ohse, E.A. Wang, J.M. Wozney, K. Yamashita, Bone morphogenetic protein-2 stimulates alkaline phosphatase activity and collagen synthesis in cultured osteoblastic cells, MC3T3-E1, Biochem. Biophys. Res. Commun. 174 (1991) 96–101. http://dx.doi.org/10.1016/0006-291X(91)90490-X.
[14] P. Ruhe, O. Boerman, F. Russel, A. Mikos, P. Spauwen, J. Jansen, In vivo release of rhBMP-2 loaded porous calcium phosphate cement pretreated with albumin, J. Mater. Sci. Mater. Med. 17 (2006) 919–927. http://dx.doi.org/10.1007/s10856-006-0181-z.
[15] O.A. Arosarena, D. Carpio-Cano, E. Fabiola, R.A. Dela Cadena, M.C. Rico, E. Nwodim, et al., Comparison of bone morphogenetic protein-2 and osteoactivin for mesenchymal cell differentiation: Effects of bolus and continuous administration, J. Cell. Physiol. 226 (2011) 2943–2952. http://dx.doi.org/10.1002/jcp.22639.
[16] E. Hunziker, L. Enggist, A. Küffer, D. Buser, Y. Liu, Osseointegration: the slow delivery of BMP-2 enhances osteoinductivity, Bone 51 (2012) 98–106. http://dx.doi.org/10.1016/j.bone.2012.04.004.
[17] J. Rui, M. Dadsetan, M.B. Runge, R.J. Spinner, M.J. Yaszemski, A.J. Windebank, et al., Controlled release of vascular endothelial growth factor using poly-lactic-co-glycolic acid microspheres: in vitro characterization and application in polycaprolactone fumarate nerve conduits, Acta Biomater. 8 (2012) 511–518. http://dx.doi.org/10.1016/j.actbio.2011.10.001.
[18] H. Hosseinkhani, M. Hosseinkhani, A. Khademhosseini, H. Kobayashi, Bone regeneration through controlled release of bone morphogenetic protein-2 from 3-D tissue engineered nano-scaffold, J. Control. Release 117 (2007) 380–386. http://dx.doi.org/10.1016/j.jconrel.2006.11.018.
[19] M. Kanatani, T. Sugimoto, H. Kaji, T. Kobayashi, K. Nishiyama, M. Fukase, et al., Stimulatory effect of bone morphogenetic protein-2 on osteoclast-like cell formation and bone-resorbing activity, J. Bone Miner. Res. 10 (1995) 1681–1690. http://dx.doi.org/10.1002/jbmr.5650101110.
[20] H. Kaneko, T. Arakawa, H. Mano, T. Kaneda, A. Ogasawara, M. Nakagawa, et al., Direct stimulation of osteoclastic bone resorption by bone morphogenetic protein (BMP)-2 and expression of BMP receptors in mature osteoclasts, Bone 27 (2000) 479–486. http://dx.doi.org/10.1016/S8756-3282(00)00358-6.
[21] M. Li, X. Liu, X. Liu, B. Ge, Calcium phosphate cement with BMP-2-loaded gelatin microspheres enhances bone healing in osteoporosis: a pilot study, Clin. Orthop. Relat. Res. 468 (2010) 1978–1985. http://dx.doi.org/10.1007/s11999-010-1321-9.
[22] P.Q. Ruhe, E.L. Hedberg, N.T. Padron, P.H. Spauwen, J.A. Jansen, A.G. Mikos, rhBMP-2 release from injectable poly (DL-lactic-co-glycolic acid)/calcium-phosphate cement composites, J. Bone Joint Surg. 85 (2003) 75–81.
[23] C. Gao, Y. Cai, X. Kong, G. Han, J. Yao, Development and characterization of injectable chitosan-based hydrogels containing dexamethasone/rhBMP-2 loaded hydroxyapatite nanoparticles, Mater. Lett. 93 (2013) 312–315. http://dx.doi.org/10.1016/j.matlet.2012.11.106.
[24] H. Shen, X. Hu, F. Yang, J. Bei, S. Wang, The bioactivity of rhBMP-2 immobilized poly (lactide-co-glycolide) scaffolds, Biomaterials 30 (2009) 3150–3157. http://dx.doi.org/10.1016/j.biomaterials.2009.02.004.
[25] M.B. Dreifke, N.A. Ebraheim, A.C. Jayasuriya, Investigation of potential injectable polymeric biomaterials for bone regeneration, J. Biomed. Mater. Res. A 101 (2013) 2436–2447. http://dx.doi.org/10.1002/jbm.a.34521.
[26] Z.S. Haidar, R.C. Hamdy, M. Tabrizian, Delivery of recombinant bone morphogenetic proteins for bone regeneration and repair. Part A: current challenges in BMP delivery, Biotechnol. Lett. 31 (2009) 1817–1824. http://dx.doi.org/10.1007/s10529-009-0099-x.
[27] O. Karal-Yilmaz, M. Serhatli, K. Baysal, B.M. Baysal, Preparation and in vitro characterization of vascular endothelial growth factor (VEGF)-loaded poly (D, L-lactic-co-glycolic acid) microspheres using a double emulsion/solvent evaporation technique, J. Microencapsul. 28 (2011) 46–54. http://dx.doi.org/10.3109/02652048.2010.523795.
[28] M. Klagsbrun, The affinity of fibroblast growth factors (FGFs) for heparin; FGF-heparan sulfate interactions in cells and extracellular matrix, Curr. Opin. Cell Biol. 2 (1990) 857–863. http://dx.doi.org/10.1016/0955-0674(90)90084-R.
[29] M. Lyon, G. Rushton, J.T. Gallagher, The interaction of the transforming growth factor-βs with heparin/heparan sulfate is isoform-specific, J. Biol. Chem. 272 (1997) 18000–18006. http://dx.doi.org/10.1074/jbc.272.29.18000.
[30] B. Zhao, T. Katagiri, H. Toyoda, T. Takada, T. Yanai, T. Fukuda, et al., Heparin potentiates the in vivo ectopic bone formation induced by bone morphogenetic protein-2, J. Biol. Chem. 281 (2006) 23246–23253. http://dx.doi.org/10.1016/j.bbapap.2012.07.002.
[31] C. Bialorucki, G. Subramanian, M. Elsaadany, E. Yildirim-Ayan, *In situ* osteoblast mineralization mediates post-injection mechanical properties of osteoconductive material, J. Mech. Behav. Biomed. Mater. 38 (2014) 143–153. http://dx.doi.org/10.1016/j.jmbbm.2014.06.018.
[32] E.D. Yildirim, D. Pappas, S. Güçeri, W. Sun, Enhanced cellular functions on polycaprolactone tissue scaffolds by O_2 plasma surface modification, Plasma Process. Polym. 8 (2011) 256–267. http://dx.doi.org/10.1002/ppap.201000009.
[33] J. Paz-Ferreiro, A. Tarquis, J. Miranda, E. Vidal Vázquez, Multiscale characterization of pore size distributions using mercury porosimetry and nitrogen adsorption, EGU General Assembly Conference Abstracts 2009, 2009, p. 12667.
[34] Y. Yeo, K. Park, Control of encapsulation efficiency and initial burst in polymeric microparticle systems, Arch. Pharm. Res. 27 (2004) 1–12. http://dx.doi.org/10.1007/BF02980037.
[35] A.S. Stephens, S.R. Stephens, N.A. Morrison, Internal control genes for quantitative RT-PCR expression analysis in mouse osteoblasts, osteoclasts and macrophages, BMC Res. Notes 4 (2011) 410. http://dx.doi.org/10.1186/1756-0500-4-410.
[36] J.W. Park, J.Y. Suh, H.J. Chung, Effects of calcium ion incorporation on osteoblast gene expression in MC3T3-E1 cells cultured on microstructured titanium surfaces, J. Biomed. Mater. Res. A 86 (2008) 117–126. http://dx.doi.org/10.1002/jbm.a.31618.
[37] Y. Tian, Y. Xu, Q. Fu, Y. Dong, Osterix is required for sonic Hedgehog-induced osteoblastic MC3T3-E1 cell differentiation, Cell Biochem. Biophys. 64 (2012) 169–176. http://dx.doi.org/10.1007/s12013-012-9369-7.
[38] J. You, G.C. Reilly, X. Zhen, C.E. Yellowley, Q. Chen, H.J. Donahue, et al., Osteopontin gene regulation by oscillatory fluid flow via intracellular calcium mobilization and activation of mitogen-activated protein kinase in MC3T3-E1 osteoblasts, J. Biol. Chem. 276 (2001) 13365–13371. http://dx.doi.org/10.1074/jbc.M009846200.
[39] I. Kanazawa, T. Yamaguchi, S. Yano, M. Yamauchi, T. Sugimoto, Metformin enhances the differentiation and mineralization of osteoblastic MC3T3-E1 cells via AMP kinase activation as well as eNOS and BMP-2 expression, Biochem. Biophys. Res. Commun. 375 (2008) 414–419. http://dx.doi.org/10.1016/j.bbrc.2008.08.034.
[40] E.D. Yildirim, R. Besunder, D. Pappas, F. Allen, S. Güçeri, W. Sun, Accelerated differentiation of osteoblast cells on polycaprolactone scaffolds driven by a combined effect of protein coating and plasma modification, Biofabrication 2 (2010) 014109. http://dx.doi.org/10.1088/1758-5082/2/1/014109.
[41] E.D. Yildirim, H. Ayan, V.N. Vasilets, A. Fridman, S. Guceri, W. Sun, Effect of dielectric barrier discharge plasma on the attachment and proliferation of osteoblasts cultured over poly(ε-caprolactone) scaffolds, Plasma Process. Polym. 5 (2008) 58–66. http://dx.doi.org/10.1002/ppap.200800047.
[42] H. Shen, X. Hu, J. Bei, S. Wang, The immobilization of basic fibroblast growth factor on plasma-treated poly(lactide-*co*−glycolide), Biomaterials 29 (2008) 2388–2399. http://dx.doi.org/10.1016/j.biomaterials.2008.02.008.
[43] T. Saito, F. Kobayashi, T. Fujii, K. Bessho, Effect of phosphophoryn on rhBMP-2-induced bone formation, Arch. Oral Biol. 49 (2004) 239–243. http://dx.doi.org/10.1016/j.archoralbio.2003.08.003.
[44] H. Uludag, D. D'Augusta, J. Golden, J. Li, G. Timony, R. Riedel, et al., Implantation of recombinant human bone morphogenetic proteins with biomaterial carriers: a correlation between protein pharmacokinetics and osteoinduction in the rat ectopic model, J. Biomed. Mater. Res. 50 (2000) 227–238.
[45] T. Takada, T. Katagiri, M. Ifuku, N. Morimura, M. Kobayashi, K. Hasegawa, et al., Sulfated polysaccharides enhance the biological activities of bone morphogenetic proteins, J. Biol. Chem. 278 (2003) 43229–43235. http://dx.doi.org/10.1074/jbc.M300937200.
[46] L.D. Quarles, D.A. Yohay, L.W. Lever, R. Caton, R.J. Wenstrup, Distinct proliferative and differentiated stages of murine MC3T3-E1 cells in culture: an in vitro model of osteoblast development, J. Bone Miner. Res. 7 (1992) 683–692. http://dx.doi.org/10.1002/jbmr.5650070613.
[47] G.R. Beck, B. Zerler, E. Moran, Phosphate is a specific signal for induction of osteopontin gene expression, Proc. Natl. Acad. Sci. 97 (2000) 8352–8357. http://dx.doi.org/10.1073/pnas.140021997.